Progress In Electromagnetics Research, Vol. 129, 51–67, 2012

SPATIAL BEAM COMPRESSION AND EFFECTIVE BEAM INJECTION USING TRIANGULAR GRADIENT INDEX PROFILE PHOTONIC CRYSTALS

N. Yogesh and V. Subramanian*

Microwave Laboratory, Department of Physics, Indian Institute of Technology Madras, Chennai-600 036, India

Abstract—Spatial beam compression of an electromagnetic wave is one of the fundamental techniques employed in microwaves and optics. As there are many ways to achieve this task using the combination of prisms and lenses, recent research suggests the parabolic gradient index photonic crystals (GRIN PC) for the design of spatial beam compressor owing to its functionalities. However, the fabrication of a graded media with the parabolic profile is a difficult challenge in practical realization. As an alternative, present work attempts this problem with respect to the triangular gradient index profile. The performance and aspects of the beam compression are investigated experimentally using the pillar type GRIN PC at the microwave length-scales. The utility of the device for an effective beam injection to the photonic-waveguide component is further demonstrated experimentally.

1. INTRODUCTION

Photonic crystals (PCs) are the periodic arrangement of dielectric constituents in one, two, and three dimensions that show various electromagnetic (e-m) phenomena including ultra-divergence, self-collimation, and negative refraction [1–5]. Gradient variations introduced in the lattice period, filling factor, and dielectric constant of these periodic media (referred as Gradient Index Photonic Crystals (GRIN PC) [6]) can provide efficient light molding applications such as spatial beam compression [7, 8], effective control over light propagation [9], optical absorbers [10], directional cloaking [11] etc.

Among several applications, spatial beam compression of an e-m wave is paid much attention, as it would be the fundamental principle

Received 2 May 2012, Accepted 27 May 2012, Scheduled 13 June 2012

* Corresponding author: Venkatachalam Subramanian (manianvs@iitm.ac.in).

for the realization of couplers in integrated and transformational electromagnetics [12–14]. The recent investigation [8] reveals the beam compression aspect of the parabolic GRIN PC lens with the index profile given as $n(r) = n_0(1 - \frac{\alpha^2}{2}r^2)$, where n_0 is the refractive index along the optical axis of the GRIN PC lens, α is the gradient coefficient (m^{-1}), and r is the geometrical coordinate (m)). The design principle of the beam compressor involves the combination of two GRIN PC lenses with different focal lengths, where the first PC focuses the parallel beam into a minimum spot size and the second lens will either collimate or diverge the minimum spot size according to the frequency dispersion.

This approach guarantees a larger beam compression ratio (input beam width to the output beam width) with respect to the frequency dependent focal lengths. However, for practical realization, one has to fabricate the parabolic graded media with the greatest precision. For example, to produce a quadratic change in the refractive index (parabolic profile), one has to produce similar change in the dimension of the PC pillars. This would be a challenging task, as the fabricating errors are larger than the actual gradation required [15].

To overcome this constraint, beam compression aspect can be studied with respect to the linear index distribution such as the triangular index profile. In a periodic media, this profile can be easily created through the linear variations in the dimension of the PC pillars. This paper reveals the aspects of the triangular index profile for the spatial beam compression and experimental investigations are carried out at the microwave length-scales. Moreover, the compressing ability of the device is utilized for the realization of effective beam injector and it is demonstrated experimentally owing to its microwave photonics applications.

2. DESIGN PARAMETERS AND NUMERICAL RESULT

2.1. Group Index Calculations

Pillar type photonic crystals consisting of square lattice arrangement of PTFE (polytetra fluoro ethylene — relative dielectric permittivity is 2.1) rods arranged in an air background is considered for the realization of the beam compressor. The investigation is done with the transverse magnetic (TM) polarization, where E-field is parallel to the axis of the pillars. To form the graded index profile, one has to compute the group index for various filling fractions. This is done with the help of plane wave expansion based open-source solver MPB [16]. The procedure is to solve for the band structure of the periodic media,

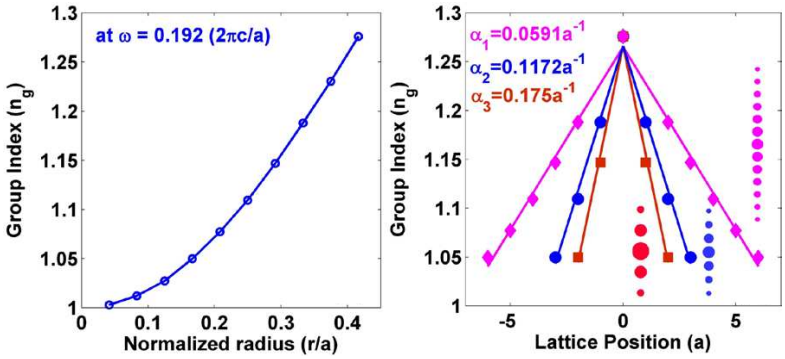

(a) (b)

Figure 1. (a) Group index as a function of the pillar radius at a normalized angular frequency of $0.192\,(2\pi c/a)$ for TM (E_z) mode polarization. (b) Triangular index profiles for various gradient coefficients at $\omega = 0.192\,(2\pi c/a)$. The diamond ($\alpha_1 = 0.0591a^{-1}$), circle ($\alpha_2 = 0.1172a^{-1}$), and square ($\alpha_3 = 0.1750a^{-1}$) markers represent the group index for the available pillar radius. For a given α, the gradation introduced along the individual vertical photonic layer is also shown in the plot.

and the group index at a given frequency is calculated through the Hellman-Feynman theorem [17].

In Figure 1(a), the group index is plotted as a function of the radius of the pillars at a normalized angular frequency of $0.192\,(2\pi c/a)$. This frequency is chosen within the homogenous response of the GRIN PC (Eigen frequency contours are circular for the pillar radius varies from $0.041667a$ to $0.41667a$) ranging from 0.18 to $0.34\,(2\pi c/a)$. If $a = 1.2\,\text{cm}$, then the radius varies from 0.05 cm to 0.5 cm and the frequency range varies within 4.5 to 8.5 GHz.

The computed group indices are fitted with the triangular index profile given as

$$n\,(r) = n_0\left(1 - \frac{\alpha}{2}\,|r|\right) \tag{1}$$

where $n(r)$ is the position dependent refractive index, 'r' is chosen along the vertical direction of the PC, and α is the gradient coefficient (m^{-1}). It may be noted that Eq. (1) is a representative of the triangular profile for a periodic media but for the modal dispersion analysis, one may need to redefine it to the other form of expressions, as discussed in fiber optics [18]. Figure 1(b) shows the triangular index fit for three different α's. Along with the theoretical fit, group indices for

the commercially available pillar radius at a given α are also shown in Figure 1(b) with the solid circles, squares and diamond markers. It may be noted that in all the three cases, the center pillar radius is taken to be 0.5 cm, which has the maximum group index value of 1.276.

2.2. Design Parameters

The result of Figure 1 is used for the formation of beam compressor. It may be noted that Ref. [8] derives the design of the parabolic GRIN PC according to the Gaussian optics approximations [19]. For example, the focal length of the parabolic GRIN PC lens is approximated to the 1/4th of the pitch length of the GRIN medium given as $f = \frac{\pi}{2\alpha}$, where 'f' is the self-focusing length of the GRIN medium and α is the gradient coefficient. This approximation is also adopted for the GRIN PC lens with the triangular index profile. It is necessary to verify the validity of such approximations for a triangular index profile. Hence, focusing length of the GRIN medium with parabolic and triangular index profile is evaluated using finite-difference time-domain based e-m solver CST MWS [20].

Figure 2 shows the focusing effect of the GRIN medium formed by the parabolic and triangular index profiles with respect to the common $\alpha = 0.1172a^{-1}$ at the frequency of 7.1 GHz. In both the cases, the GRIN medium has 31 rows with the lattice period of $a = 1.2$ cm. Plane wave excitation is used for the computation and perfectly matched boundary condition [21] is employed around the computational domain to terminate the open space.

Figures 2(a) and (b) show the focusing effect for the parabolic GRIN medium at 7.1 GHz, where the focal length calculated from the electric field intensity profile is found to be around 15.9 cm. Similarly, for the triangular GRIN medium (given in 2(c) and (d)) the focal length is found to be around 17.1 cm. Both these values are closer to the theoretical value ($f = \frac{\pi}{2\alpha}$) of 16.08 cm for a given $\alpha = 0.1172a^{-1}$, where 'a' is taken to be 1.2 cm. Hence, the focal length approximation used for the parabolic GRIN PC may also be taken for the triangular GRIN PC for further analysis.

The beam compressor investigated in this work is shown in Figure 3. It involves a combination of two GRIN PC lenses, where PC1 is graded with the $\alpha_{PC1} = 0.1172a^{-1}$ and PC2 is graded with the $\alpha_{PC2} = 0.175a^{-1}$. The explicit position of the pillar radius and its variation is also given in Figure 3. The lengths of the PC1 and PC2 are chosen using $f = \frac{\pi}{2\alpha}$, where PC1 has a length of $13a$ and PC2 has a length of $9a$ respectively.

2.3. Numerical Results

The beam compression aspect of the design given in Figure 3 is studied using the finite-element method (FEM) based e-m solver FEMLAB [22]. Figure 4 shows the results of the frequency dependent beam compressibility with respect to the different input beam apertures.

For the first case, the compression is probed for a finite aperture size of 7.2 cm (an arbitrary choice). The E_z field map given at 4.8 GHz in Figure 4(a) and full-width half-maximum (FWHM) values of the

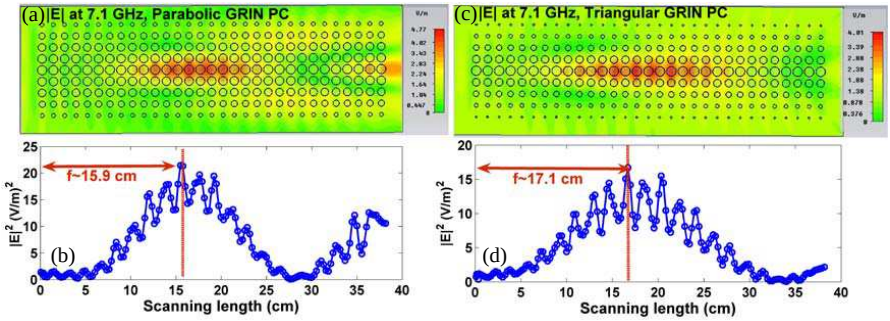

Figure 2. (a) and (b) show the focusing and the corresponding scanning plot of the parabolic GRIN medium. (c) and (d) show the focusing and the scanning plot for the triangular index GRIN medium. Both use a gradient coefficient of $\alpha = 0.1172a^{-1}$ at 7.1 GHz.

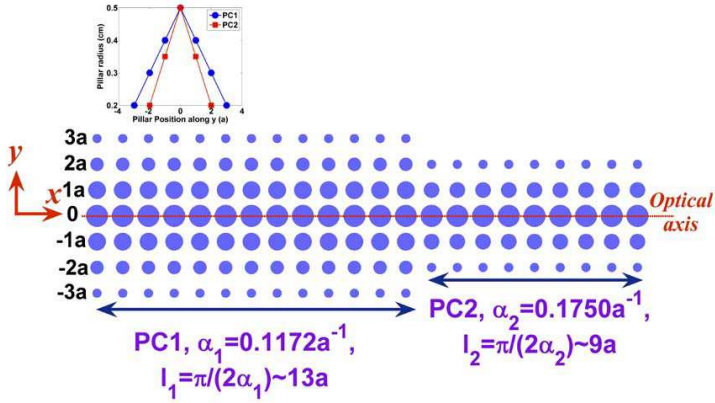

Figure 3. Design of beam-aperture modifier with respect to the triangular index profile. Explicit position of the pillars and its radius variation is given in the inset.

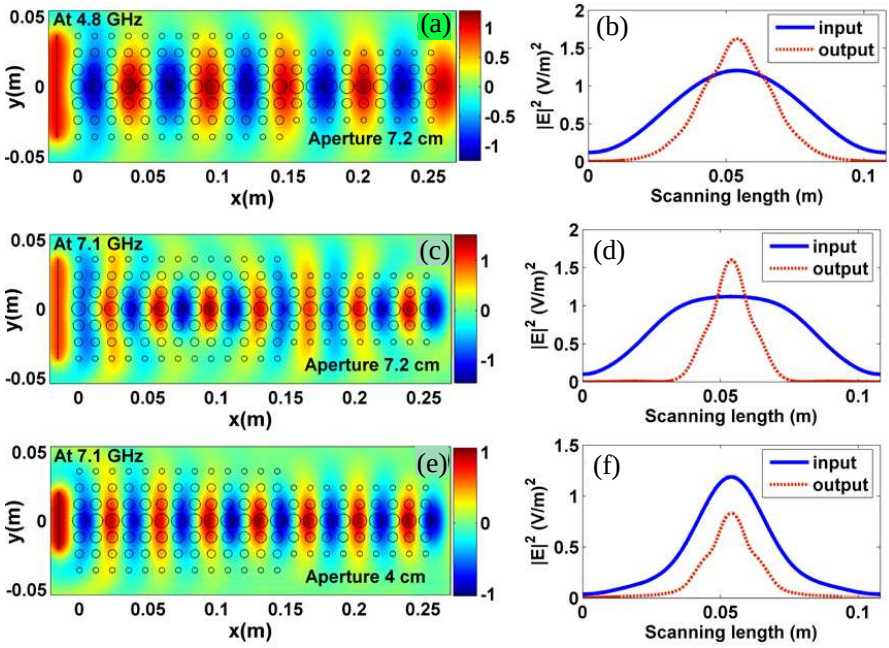

Figure 4. (a) E_z field map at 4.8 GHz for the finite aperture size of 7.2 cm and (b) shows the corresponding electric field intensity profiles at the input (i/p)/output (o/p) planes. (c) E_z field map at 7.1 GHz for the aperture size of 7.2 cm and (d) shows the corresponding $|\mathrm{E}|^2$ profiles of the i/p and o/p beams. (e) E_z field map at 7.1 GHz for the aperture size of 4 cm and (f) shows the corresponding $|E|^2$ profiles of the i/p and o/p beams.

input/output electric field intensity ($|E|^2$) profiles shown in Figure 4(b) reveal the spatial beam compression ratio around 2 : 1. On the other hand, for the same aperture size, the E_z field map given at 7.1 GHz in Figure 4(c) and FWHM of the input/output $|E|^2$ profiles (Figure 4(d)) show the compression ratio around 4 : 1. According to Ref. [8], for the given gradient coefficients ($\alpha_{PC1} = 0.1172a^{-1}$ and $\alpha_{PC2} = 0.175a^{-1}$), one should expect the beam compression ratio $\left(\frac{\alpha_{PC2}}{\alpha_{PC1}}\right)$ around 1.5 : 1. However, this empirical ratio does not taken into account of the frequency dispersion condition, where the effective focal length of the system is frequency dependent.

For example, as per the Gaussian optics approximations, GRIN lens with the focal length 'f' will change the incident beam width (W_0)

into the output beam width of W_1 as

$$W_1 = \frac{\lambda f}{\pi W_0} \tag{2}$$

here λ is the applied wavelength. By substituting the values of W_1 and W_0, one can retrieve the effective focal length of the configuration as 8.1 cm at 4.8 GHz and 7.3 cm at 7.1 GHz respectively. On the other hand, the frequency independent equation for the combined focal length of the configuration can be written as

$$f = \frac{f_1 f_2}{f_1 + f_2} \tag{3}$$

Here f_1 and f_2 are the focal lengths of the GRIN PC1 and GRIN PC2 defined according to the plane wave (no finite aperture) approximation as $f = \frac{\pi}{2\alpha}$, where α is the gradient coefficient. The approximated value of $f_1 = 13a$ and $f_2 = 9a$ yields the combined focal length of 6.4 cm as per Eq. (3). This comparison reveals the frequency dependent characteristic of the GRIN PC lens and the higher beam compressibility is attributed to the entrance aperture effect.

For the second case, the beam compression is probed with respect to size of the input beam aperture. The E_z field map given in Figure 4(e) at 7.1 GHz reveals the compression effect for a smaller beam aperture of size 4 cm. Unlike in Figure 4(c), the focusing effect is not dominant in Figure 4(e) and this will result in reduced beam compression ratio of 1.76 (Figure 4(f)). This is in accordance with the Eq. (3), where input beam width plays major role in the beam compression aspect.

To verify the above numerical results, two different microwave apertures are considered in the experimental demonstration. J-band (4.5 to 8.2 GHz) and the X-band (6.8 to 8.5 GHz) horn antennas are used for the excitation of larger input beam-widths. Passive waveguides are considered as the sources for the smaller beam apertures.

3. EXPERIMENTAL INVESTIGATIONS

Beam compressor design given in Figure 3 is fabricated using PTFE rods and the experimental set up is given in Figure 5. The measured (using Transmission-Reflection line method [23]) dielectric constant of the PTFE is $\varepsilon_r = 2.001 - j0.006$. Height of the rods is taken to be 10 cm and this choice ensures the reduction in the out-of-plane radiation losses due to the finite third dimension of the PC (It may be noted that in optical length-scales, reasonable estimation on the

choice of the height of the PC slab is available for effective vertical confinement mechanisms [24]). The rods were arranged in a square lattice symmetry with the periodicity of $a = 1.2\,\text{cm}$.

The beam scanning measurements are carried out with vector network analyzer (N5230A). The beam coming from the J-band horn antenna is given as an input to the GRIN PC and the antenna is placed behind the beam compressor as shown in Figure 5(a). Monopole attached to the coaxial cable is used as the detector and it is mounted on a Vernier microscope for beam scanning. The beam compression aspect for a larger beam aperture given in Figure 5(b) shows the input/output FWHM profiles for 7.1016 GHz. It is evident that the ratio of the input beam width (8.370 cm) to the output beam width (2.640 cm) is around 3.2 at 7.1016 GHz.

The beam compression ratio for other range of frequencies (4.5 to 8 GHz) is given in Figure 5(c). It is clear that for a larger beam aperture (given with blue open circles), the compression ratio is found

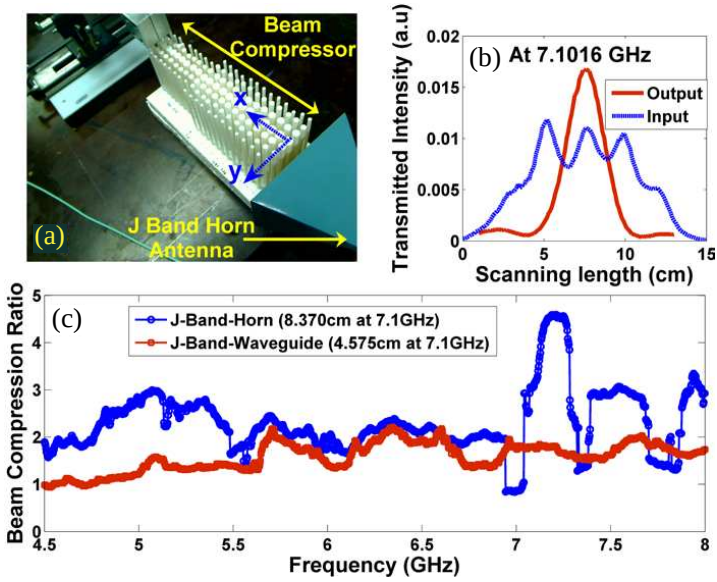

Figure 5. (a) Experimental setup for the beam compression studies. (b) Transmitted intensity profiles of the input and output beam scanned at 7.1016 GHz. (c) Beam compression ratio over a working frequency range of 4.5 to 8 GHz. Blue circled line corresponds to a larger beam aperture (J-band horn) and the red squared line corresponds to a smaller beam aperture (J-band waveguide).

in-between 2 : 1 to 4 : 1. The larger value obtained at the higher frequencies reveals the entrance aperture effect and importantly the frequency dispersive characteristics of the GRIN PC lens.

On the other hand, for a smaller beam aperture (given with red open squares), the compression ratio is found to be around 1 : 1 for the range 4.5 to 5.5 GHz and 2 : 1 for the range 6 to 6.9 GHz. In case, if an input beam width matches to that of the GRIN PC mode, one can expect the self-collimation phenomenon, where the beam width is undistorted over the entire device [7]. The beam compression ratio of 1 : 1 observed in Figure 5(c) reveals the domination of collimation effect, where the e-m beam is confined and guided along the optical axis due to the higher refractive index.

4. APPLICATION — ELECTROMAGNETIC BEAM INJECTOR

The utility of this beam compression aspect can be explored with respect to an effective beam injection in microwave photonic devices. Injecting an e-m beam from free space or from a source component to any guiding medium is an inevitable task in many branches of microwave and optics. The common objective is to improve the coupling efficiency, reducing the return losses and increasing the operational bandwidth. There have been different mechanisms to achieve the above task and in particular, the following three are reported based on the photonic crystals;

1 PC concave lens configuration [12] — This approach utilizes the negative refraction concept in PC concave lens so that the larger size beam width can be focused on to a waveguide device with the sub-wavelength focusing. Disadvantages are the limited bandwidth of negative refraction and aberrations due to the geometrical curvature.

2 Tapered Waveguide [13] — It accompanies the introduction of gradient tapers in the PC waveguides for the effective coupling of an input beam. This approach has a constraint on the nature of the source and its beam width, but for most of the laser applications, this approach is sufficient.

3 GRIN PC coupler [14] — This approach is based on the concept of strong focusing effect of the single gradient lens for the effective coupling in a waveguide device.

Among the three different approaches, the graded index approach gives the promising features of a coupling element. It is important to note that as in Ref. [14], single graded lens itself suffices to show

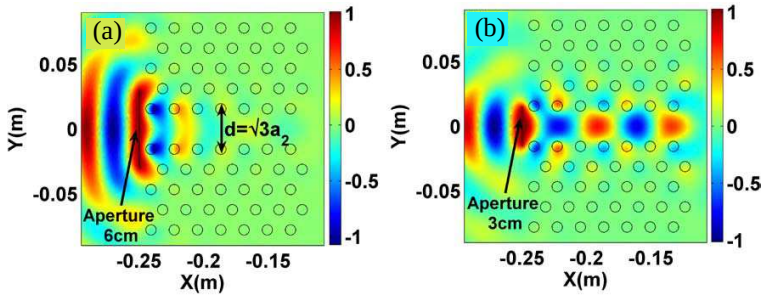

Figure 6. The role of source aperture for an effective-beam injection in a photonic crystal waveguide. (a) E_z field map at 7.5 GHz corresponds to the source's aperture of 6 cm. (b) E_z field map at 7.5 GHz to the source aperture of 3 cm. The PC waveguide is formed by the removal of center of row of rods in a 14×11 layers of triangular lattice photonic crystal (defect spacing is $d = \sqrt{3}a_2$, where 'a_2' is the lattice constant taken to be 1.8 cm).

the effective beam injection, but it is specially targeted for a single frequency operation. On the other hand, the aperture modifier dealt in this work is looked for the effective beam injection over a range of beam-compressing frequencies and their functionalities are probed experimentally at the microwave length-scales.

4.1. Numerical Results

To demonstrate the coupling aspect of the beam compressor, PC waveguide shown in Figure 6(a) is considered. It is made of triangular lattice arrangement of glass rods (relative dielectric constant of $\varepsilon_r = 5.5$) of radius $r = 0.4$ cm and with the lattice periodicity of $a_2 = 1.8$ cm. Removing the center row of rods will form the waveguide with the defect spacing of $\sqrt{3}a_2$ and confines the e-m wave corresponding to the defect-band frequencies ranging from 6.38 to 8.33 GHz.

Figure 6 reveals the importance of the problem, as it shows the E_z field map at 7.5 GHz (a) for a larger beam aperture of 6 cm and (b) for a smaller aperture of 3 cm. It is evident that the larger beam width does not couple to the PC waveguide, as most of the power is reflected back from the PC waveguide itself. On the other hand, when an incident beam width matches to that of PC waveguide width, the e-m beam is steered in to the waveguide. Hence, it is clear that the source with larger aperture cannot be integrated to any photonic device unless its spatial width is compressed. For an example, the

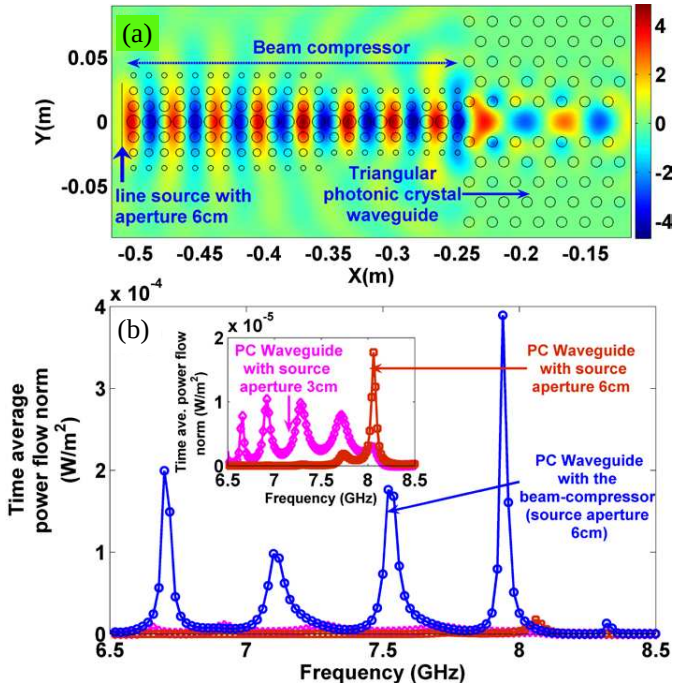

Figure 7. Numerical result of an effective beam injection. (a) E_z field map at 7.5 GHz shows the effective coupling provided by the beam compressor for a source aperture of 6 cm. (b) Time-averaged power flow norm is plotted for the configurations of empty PC waveguide with source apertures of 6 and 3 cm (given in the inset), and the PC waveguide with the beam compressor for the source aperture of 6 cm.

directional cloaking device discussed in Ref. [25] is functional only with the introduction of a beam compressor. Otherwise, the concept of invisibility or transparency is lost due to the under coupling effect of the incident e-m wave to the PC waveguide.

The role of beam compressor in effective beam injection is given in Figure 7. The E_z field map given at 7.5 GHz for a larger beam aperture (6 cm) (Figure 7(a)) shows the smooth steering of e-m beam into the PC waveguide.

In Figure 7(b), the transmitted time-averaged power flow norm (It is the modulus value of the Poynting vector) is plotted for all the three cases (PC waveguide without the beam compressor for larger and smaller beam apertures (given in inset of Figure 7(b)) and PC waveguide with the beam compressor for a larger beam aperture).

It is witnessed that the insertion of beam compressor between the source and the PC waveguide results in enhanced power flow, as the compressor produce the light transformation with the compressed beam width. In order to have further information on the effective coupling result, an experiment is conducted at the microwave length-scales.

4.2. Experimental Setup and Measurements

The PC waveguide part is fabricated using the glass rods with the radius of 0.4 cm arranged in triangular lattice symmetry with the periodicity of 1.8 cm. The measured dielectric permittivity of glass rods is found to be $\varepsilon_r = 5.847 - j0.077$. Height of the glass rods is taken to be 10 cm. The complete experimental setup is shown in Figure 8 and the scattering parameters (relative reflection and relative transmission) are measured using the vector network analyzer (N5230A). The relative scattering parameters are defined as follows

$$(S_{21})_{relative} = (S_{21})_{structure} - (S_{21})_{freespace}$$
$$(S_{11})_{relative} = (S_{11})_{structure} - (S_{11})_{freespace}$$

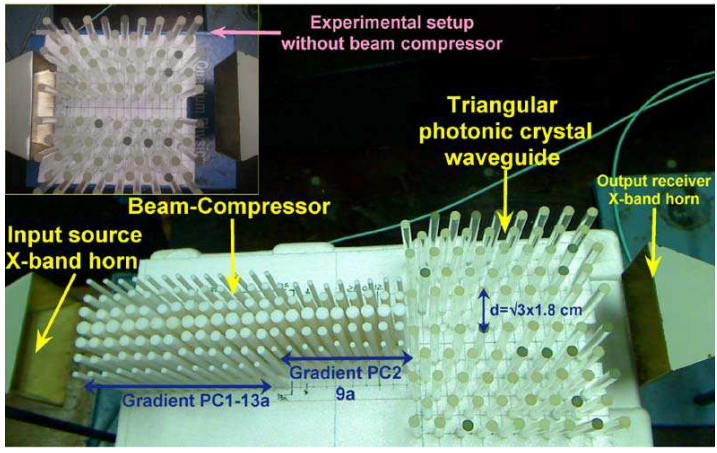

Figure 8. Experimental setup for an effective beam injection. The beam compressor has a length of 26.4 cm, and the PC waveguide has a length of 14.4 cm. This picture shows the X-band horn as the transmitter and receiver. Inset of the figure shows the setup for an empty PC waveguide.

$$S_{21} = 20\log_{10}\left(\frac{E_{transmitted}}{E_{incident}}\right)$$
$$S_{11} = 20\log_{10}\left(\frac{E_{reflected}}{E_{incident}}\right) \quad (4)$$

In Eq. (4), $(S_{21})_{strucuture}$ is the measured transmitted power (dB scale) in the presence of photonic structure, $(S_{21})_{freespace}$ is the measured transmitted power (dB scale) in the free space, and S_{21} and S_{11} are the general definition of the transmitted and reflected power (dB scale) respectively. Figure 9 shows the plot of relative parameters for various available beam apertures such as X-band horn antenna, X-band waveguide, and J-band horn antenna.

4.3. Results and Discussions

The first part of the result (given in Figures 9(a) and 9(d)) shows the relative parameters for the beam injection from a X-band horn antenna. The beam width of an input beam measured at 2 cm away from the X-band horn is found to be around 4–5 cm in the frequency range of 7 to 8 GHz. By comparing the relative transmission of PC waveguide with ((blue solid line in Figure 9(a)) and without the beam compressor (red dashed line in Figure 9(a)), an improvement of 5 to 15 dB transmission is observed in the frequency range of 7 to 8 GHz. In order to have clear idea about the beam injection, one can take one of the frequencies in Figure 9(a) and Figure 9(d) (indicated by arrows). At 7.263 GHz, PC waveguide shows the transmission loss of around 17 dB with respect to free space, whereas with the introduction of the beam compressor, the transmission loss is only around 5 dB with respect to the free space. For the return loss part (in Figure 9(d)), it is found that the PC waveguide without the beam compressor is approximately 13 dB more reflective than the PC waveguide with the beam compressor at 7.263 GHz.

The second part of the result (given in Figures 9(b) and 9(e)) considers the beam injection with respect to the larger beam aperture (J-band horn). Since the investigated beam compressor is not sufficient to accommodate the entire wavefront, an improved transmission of 8 to 12 dB is observed only in the shaded regimes. Moreover, the relative reflected spectrum given in Figure 9(e) reveals the higher reflectivity with respect to the free space. It is useful to mention that the beam compressor is designed only based on the commercially available rod's diameters. In case, if one further increases the rod layers along the transverse direction, the entire wavefront can be accommodated within the GRIN PC and this will also ensure the accurate representation of the triangular-index profile (one can compare the theoretical and practically realizable profiles in Figure 1(b)).

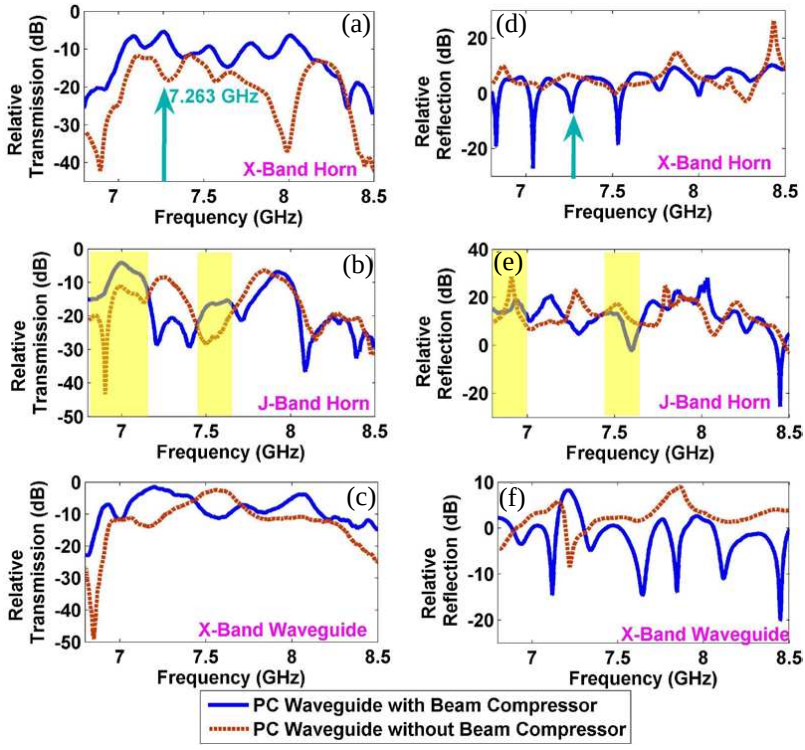

Figure 9. (a)–(c) shows the relative transmission parameter and (d)–(f) shows the relative reflective parameter for the PC waveguide with (blue solid line) and without (red dashed line) the beam compressor for the apertures of X-band horn antenna, J-band horn antenna, and X-band waveguide. The term 'relative' refers to the comparative transmission/reflection value between the structure and an air background.

The third part of the result considers the effect of a smaller beam aperture. Though the device is not efficient for a smaller beam aperture, the collimation effect may be sought for the beam injection owing to its divergence less beam propagation. Figures 9(c) and 9(f) shows an effective beam injection with an improved transmission of around 10 dB within the frequency range of 6.8 to 8 GHz. However, it is important to mention that for a smaller beam-aperture, the empty PC waveguide may be sufficient, when the source aperture matches to that of PC waveguide mode.

5. CONCLUSIONS AND PERSPECTIVES

Triangular index profile GRIN PC is emphasized for the design of spatial beam compressor, as the parabolic profile is difficult to realize practically. Focusing characteristics of the triangular index GRIN PC is evaluated numerically. It is demonstrated that the frequency dependent focal lengths and the finite beam aperture play major roles in the beam compression aspect. The following results are verified experimentally at the microwave length-scales using the PTFE pillar type PC. For a larger beam-aperture, the beam compression ratio of 2 : 1 is observed at the J-band frequencies. Higher beam compression is attributed to the frequency dispersion characteristics and entrance aperture effect of the GRIN PC lens. The beam compression ratio 1 : 1 suggests the collimation effect, as the light beam is guided and undistorted over the entire device. This will happen, when an incident beam width is matched to that of the GRIN PC mode. The utility of the device for effective beam injection is investigated both numerically and experimentally. The experimental results reveal the promising features of the beam compressor, where it injects the larger spatial width e-m beams into the photonic waveguide devices with an improved transmission of 10 dB. It is observed that the investigated design also has some limitations with respect to the wavefront size, out-of-plane radiation losses, approximated triangular index profile due to the non-availability of the rods etc. It is expected that the optimization of this effective beam injector will be useful for some of the transformational and integrated electromagnetic applications such as directional cloaking, inter-connectors, transitions etc.

REFERENCES

1. Yablonovitch, E., "Inhibited spontaneous emission in solid state physics and electronics," *Phys. Rev. Lett.,* Vol. 58, No. 20, 2059–2062, 1987.
2. Kosaka, H., T. Kawashima, A. Tomita, M. Notomi, T. Tamamura, T. Sato, and S. Kawakami, "Superprism phenomena in photonic crystals," *Phys. Rev. B*, Vol. 58, No. 16, R10096, 1998.
3. Kosaka, H., T. Kawashima, A. Tomita, M. Notomi, T. Tamamura, T. Sato, and S. Kawakami, "Self-collimating phenomena in photonic crystals," *Appl. Phys. Lett.*, Vol. 74, No. 9, 1212, 1999.
4. Yogesh, N. and V. Subramanian, "Analysis of self-collimation based cavity resonator formed by photonic crystal," *Progress In Electromagnetics Research M*, Vol. 12, 115–130, 2010.
5. Luo, C., S. G. Johnson, J. D. Joannopoulos, and J. B. Pendry,

"All-angle negative refraction without negative effective index," *Phys. Rev. B*, Vol. 65, No. 20, 201104(R), 2002.

6. Centeno, E. and D. Cassagne, "Graded photonic crystals," *Opt. Lett.*, Vol. 30, No. 17, 2278–2280, 2005.
7. Kurt, H. and D. S. Citrin, "Graded index photonic crystals," *Opt. Exp.*, Vol. 15, No. 3, 1240–1253, 2007.
8. Lu, M., B. K. Juluri, S.-C. S. Lin, B. Kiraly, T. Gao, and T. J. Huang, "Beam aperture modifier and beam deflector using gradient-index photonic crystals," *J. Appl. Phys.*, Vol. 108, No. 10, 103505, 2010, Supplementary material at http://dx.doi.org/10.1063/1.3499630.
9. Ren, K. and X. Ren, "Controlling light transport by using a graded photonic crystal," *Appl. Opt.*, Vol. 50, No. 15, 2152–2157, 2011.
10. Wang, H.-W. and L.-W. Chen, "A cylindrical optical black hole using graded index photonic crystals," *J. Appl. Phys.*, Vol. 109, No. 10, 103104, 2011.
11. Vasi, B. and R. Gaji, "Self-focusing media using graded photonic crystals: Focusing, fourier transforming and imaging, directive emission, and directional cloaking," *J. Appl. Phys.*, Vol. 110, No. 5, 053103, 2011.
12. AbdelMalek, F., W. Belhadj, S. Haxha, and H. Bouchriha, "Realization of a high coupling efficiency by employing a concave lens based on two-dimensional photonic crystals with a negative refractive index," *J. Lightw. Technol.*, Vol. 25, No. 10, 3168–3174, 2007.
13. Chien, H.-T., C. Lee, H.-K. Chiu, K.-C. Hsu, C.-C. Chen, J. A. Ho, and C. Chou, "The Comparison between the graded photonic crystal coupler and various couplers," *J. Lightw. Technol.*, Vol. 27, No. 14, 2570–2574, 2009.
14. Cakmak, A. O., E. Colak, H. Caglayan, H. Kurt, and E. Ozbay, "High efficiency of graded index photonic crystal as an input coupler," *J. Appl. Phys.*, Vol. 105, No. 14, 103708, 2009.
15. Moore, D. T., "Gradient-index optics: A review," *Appl. Opt.*, Vol. 19, No. 7, 1035–1038, 1980.
16. Johnson, S. G. and J. D. Joannopoulos, "Block-iterative frequency-domain methods for Maxwell's equations in a plane wave basis," *Opt. Exp.*, Vol. 8, No. 3, 173–190, 2001, http:/ab-initio.mit.edu/mpb.
17. Sakoda, K., *Opitcal Properties of Photonic Crystals*, Chapter 2.5, 30–34, Springer, 2005.
18. Chen, C.-L., *Foundations for Guided-wave Optics*, Chapter 9, 226,

Wiley, 2007.

19. Roux, F. S. and I. De Leon, "Planar photonic crystal gradient index lens, simulated with a finite difference time domain method," *Phys. Rev. B.*, Vol. 74, No. 11, 113103, 2006.
20. More information can be found at http://www.cst.com.
21. Taflove, A. and S. C. Hagness, *Computational Electrodynamics the Finite-difference Time-domain Method,* 3rd Edition, Chapter 7, 273–327, Artech House, Boston, 2005.
22. Whiteman, J. R., *The Mathematics of Finite Elements and Applications,* John Wiley and Sons, Chichester, 1998, http://www.comsol.com.
23. Jarvis, J. B., E. J. Vanzura, and W. A. Kissick, "Improved technique for determining complex permittivity with the transmission/reflection method," *IEEE Trans. Microwave Theory Tech.*, Vol. 38, No. 8, 1096–1103, 1990.
24. Johnson, S. G., S. Fan, P. R. Villeneuve, and J. D. Joannopoulos, "Guided modes in photonic crystal slabs," *Phys. Rev. B*, Vol. 60, No. 8, 5751–5758, 1999.
25. Yogesh, N. and V. Subramanian, *Directional Cloaking Formed by Photonic Crystal Waveguides,* accepted for presentation in International Microwave Symposium 2012, Montreal, Canada, Jun. 16–21, 2012.